Quantitative Thermal Analysis of Transient Liquid-Phase-Sintered Cu-Ni Powders

D.M. TURRIFF and S.F. CORBIN

Differential scanning calorimetry (DSC) was used to study the transient liquid phase sintering (TLPS) of elemental Ni and Cu powder mixtures. The initial melting behavior, kinetics of isothermal solidification, and remelt behavior of these powder mixtures were quantified, using DSC and metallographic techniques. The effects of the initial liquid distribution and processing temperature on these events were investigated. Quantitative DSC analysis indicates that suppressed liquid fractions form during TLPS at peak temperatures of 1090 °C and 1140 °C, due to solid-state interdiffusion prior to melting. Larger liquid fractions form at 1140 °C compared to 1090 °C, due to the recovery of some liquid previously lost to interdiffusion by dissolution at the higher peak temperature. This resulted in higher sintered densities at 1140 °C. Complete isothermal solidification of the Cu-rich transient liquid requires more time at 1140 °C due to higher liquid fractions initially formed at this temperature compared to those formed at 1090 °C. When the initial liquid is distributed nonuniformly, isothermal solidification times are also longer. The DSC and metallographic data indicate that the transient liquid phase (TLP) isothermally solidifies by limited long-range Cu diffusion into the Ni particles and by the epitaxial growth of a surrounding Cu-rich "layer" *via* the gradual outward progression of the solid/liquid interface at compositions given by the liquidus and solidus.

I. INTRODUCTION

TRANSIENT liquid phase (TLP) processing has received considerable interest in a wide range of applications, including lower-temperature soldering in the microelectronics industry,[1–7] high-temperature brazing using traditional and wide-gap transient liquid phase bonding (TLPB)[8,9] and transient or supersolidus liquid phase sintering (TLPS/SLPS) of bulk materials as well as of brazes.[10–14] In TLPS, the transient liquid that forms during sintering, aids in rapid densification of the powder compact.[15] This liquid alloys with the base metal powder during sintering, and this can lead to isothermal solidification and a shifted melting point for the mixture.

When TLPS technology is applied to braze pastes consisting of mixed powders, it can offer a number of advantages including the following: (1) a reduction in the braze temperature required to form a liquid phase; (2) rapid densification *via* the liquid's capillary action; (3) liquid removal at the process temperature by diffusional (or isothermal) solidification; (4) variable melting point (VMP) behavior due to *in-situ* alloying, which allows stepwise brazing; and (5) increased microstructural homogeneity by avoiding the formation of detrimental nonequilibrium phases and a cast structure

D.M. TURRIFF, Postdoctoral Fellow, and S.F. CORBIN, Professor, are with the Department of Mechanical Engineering, University of Waterloo, Waterloo, ON, Canada. Contact e-mail: dmturrif@engmail.uwaterloo.ca

that would otherwise form due to athermal solidification upon cooling.[5–8,15,16]

In the context of a TLPS-VMP braze, the amount of liquid initially formed during TLP processing is particularly important, as it should be sufficient to densify the braze and bond the faying surfaces of the substrates to be joined, yet isothermally solidify within a reasonable, known time frame. Base metal particle size (a_B),[7,17–19] relative diffusivities (D),[18,20] base metal grain size (d),[18] heating rate (R_H),[7,14,17,19,21] processing temperature (T_P),[12,14,17,19,21] base/additive solubilities,[17,21] powder purity and morphology,[17] and bulk alloy composition[7,12–14,19] have all been found to significantly influence the amount of liquid formed and its duration during TLPS.[5–7,17,19] In turn, the amount and duration of the liquid phase critically affects densification.[5,13,19,21] The sensitivity of TLPS to these variables has been typically investigated by dilatometry, chemical analysis, and metallographic analysis techniques.[1–4,10–13,22] These methods provide useful information regarding the sintering behavior of TLPS powder systems in regard to bulk dimensional changes or microstructural evolution for isolated particles within complex powder mixture specimens, but it is not possible to determine quantitatively the amount of liquid formed and its transient nature during sintering, using these *ex-situ* techniques. In addition, a quantification of the kinetics of liquid removal (or isothermal solidification) has received little attention.

The primary goal of this investigation was to develop an experimental technique based on differential scanning calorimetry (DSC), to characterize quantitatively

the different stages of TLPS: focusing on initial liquid formation, isothermal solidification kinetics, and remelt behavior. Particular emphasis is placed on the role that solid-state interdiffusion prior to melting and dissolution during melting play in liquid formation.

II. MATERIALS AND METHODS

The Cu-Ni binary isomorphous system was chosen for this investigation, because it both represents a simple model system for TLPS and has practical importance as a commercially-viable, VMP braze material. The copper powder represents the low-melting-point additive phase (*i.e.*, $T_m = 1085$ °C) and the source of liquid during sintering. The Ni powder represents the high-melting-point (*i.e.*, $T_m = 1455$ °C) base metal phase. Table I lists the powders used and their relevant characteristics. The average particle size of the Ni powder was determined *via* optical microscopy, due to its excessive size. Each powder was stored in a nitrogen chamber prior to use, in order to avoid long-term oxidation.

As pointed out by Lal *et al.*,[14] both the liquid content and its distribution, as a function of sintering temperature and time, are controlling features during TLPS. In this investigation, sintering temperatures of 1090 °C (*i.e.*, just past the melting point of pure Cu) and 1140 °C were explored. In all cases, a heating and cooling rate of 40 °C/min was used. Initial liquid content was varied by a change in the bulk composition of the mixtures (C_O) from 35 to 75 wt pct Cu. However, after a preliminary liquid formation and densification study, the remainder of the work focused on a Ni-65 wt pct Cu composition. Initial liquid distribution was varied, using two preparation techniques (type A and type B).

In type A (layered/pressed powders), Cu and Ni powders were individually poured directly into a die in the correct proportion and then uniaxially pressed at 165 MPa, to form 100-mg, layered disk-shaped compacts 4.75 mm in diameter. This created a Cu powder layer, which was poorly distributed among the Ni powder and was, therefore, a segregated liquid distribution.

In type B (loose/mixed powder mixtures), Cu and Ni powders were mixed to the desired bulk composition (C_O) and milled for 1 hour. This created a well-distributed Cu powder among the Ni powders which would, in turn, lead to a well-distributed initial liquid.

In addition to the two heating profiles just described, some samples were heated just below the Cu melting point (1075 ± 5 °C) and cooled, to observe the solid-state-sintered "premelt" structure. A selection of samples that had already been sintered were also reheated to 1300 °C, to characterize the degree of homogeneity and increased melting temperature due to the sintering process.

Samples of these mixtures that had a 100-mg total mass were placed in Al_2O_3 crucibles (5 mm in diameter and 5 mm tall) for sintering in the differential scanning calorimeter, which used a N_2 purge gas. Experiments were performed using a temperature and enthalpy calibrated heat-flux Netzsch* 404C DSC. The DSC

---

*Netzsch is a trademark of Alfa Aesar®, Ward Hill, MA.

---

specimens were mounted and polished perpendicular to the disk-shaped plane, to show through thickness variations using conventional metallographic techniques. Backscattered electron (BSE) images and quantitative energy-dispersive X-ray spectroscopy (EDS) line scans were collected, in order to distinguish between the interdiffused Ni- and Cu-rich regions of the postsintered DSC specimens.

III. RESULTS AND ANALYSIS

In the following subsections, the results will be presented systematically according to the stages of TLPS, namely: (1) solid-state sintering, (2) melting/dissolution, (3) isothermal solidification, and (4) homogenization. A description of important TLPS stages in liquid-rich Ni-Cu systems is described elsewhere.[23]

A. Solid-State Sintering and Diffusion

Figure 1 illustrates a macrograph of Ni-65 wt pct Cu powder mixtures made by the type A and type B methods, after heating to 1075 °C and then cooling. The different distribution of Cu powder within the Ni powder in the two mixing cases is clearly visible, as is the relatively low density of the powder compacts prior to liquid formation. Figure 2 shows an isolated Ni-Cu contact from the type A mixture after solid-state sintering at 1075 °C. The EDS line scans for Cu and Ni clearly indicate that significant diffusion of Cu into Ni particles (and *vice versa*) has occurred in the sintered neck regions. The interdiffusion region on the Cu-rich side of the sintered neck will not melt if heated to 1085 °C, because any Ni alloying of pure Cu increases its solidus temperature.

Table I. Powder Data

Powder	Purity (Metals Basis)	Mesh Size	Average Size ($d/2$)	Shape	Supplier
Cu	99.9 pct < 1000 ppm O	−170 + 400	23.09 μm*	spherical**	Alfa Aeser
Ni	99.90 pct	−48 + 150	80.50 μm**	spherical**	Alfa Aeser

* Horiba CAPA-700 particle size analyzer.
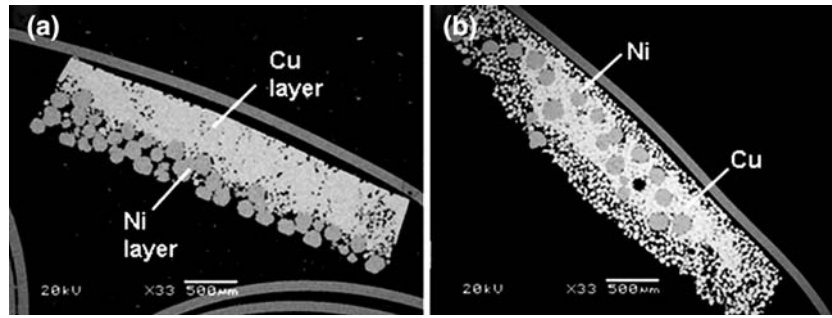** Verified *via* optical microscopy, SEM.

Fig. 1—BSE micrographs of Ni-65 wt pct Cu powder mixtures heated to 1075 °C and immediately cooled, to illustrate the premelt condition of both techniques: (a) type A (layered/pressed) and (b) type B (mixed/loose).
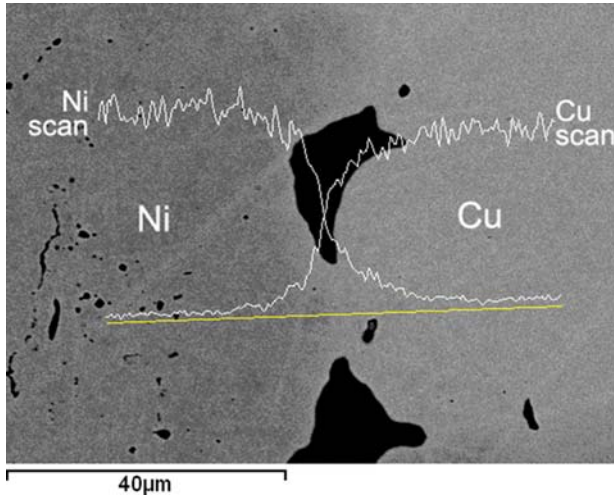

Fig. 2—BSE micrograph with qualitative EDS line scans of a Ni-65 wt pct Cu powder mixture heated to 1075 °C.

Fig. 3—DSC traces showing initial melting endotherms for layered/pressed brazes (type B) heated to 1140 °C with varying Cu contents.

B. Melting and Dissolution

The extent of solid-state interdiffusion illustrated in Figure 2 can be quantified using DSC by examining the initial liquid formation, because significant levels of solid-state interdiffusion during heating should cause a measurable suppression of the liquid volume formed. Figure 3 shows DSC heat flow traces for Cu-Ni mixtures having different bulk Cu contents (C_O) that were heated to 1140 °C and immediately cooled. The endothermic peaks found upon heating indicate that the onset of melting occurred at 1085 °C (i.e., pure Cu melting). The variation of peak areas indicate that the initial amount of liquid formed increases as the bulk Cu content of a mixture increases, which would be expected.[7,12–14] The initial liquid weight fraction formed from additive melting (W_{Ao}) can be determined by measuring the area under the endothermic peaks and dividing this measured endothermic energy (ΔH_m) by the expected endothermic energy, if the sample was 100 pct Cu (i.e., the latent heat of fusion, ΔH_f, for Cu), as per Eq. [1].
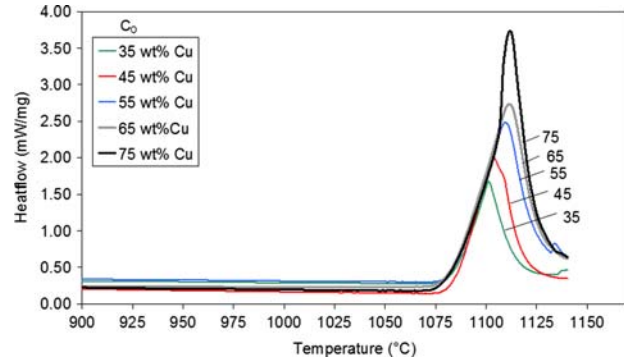
$$W_A = \frac{\Delta H_m}{\Delta H_f} \qquad [1]$$

The latent heat of fusion value (ΔH_f) for the pure Cu powder of Table I was measured by DSC under identical experimental conditions as the mixtures. In the absence of solid-state interdiffusion, all of the Cu in the sample should melt in its pure form when heated above 1085 °C. In this case, the initial liquid fraction (W_{Ao}) would be equal to the Cu content in the mixture (C_O). Therefore, the degree to which the experimentally-measured $W_{Ao} < C_O$ is a measure of how much interdiffusion took place prior to melting. A summary of ΔH_m and ΔH_f values measured via DSC (for mixtures and pure Cu, respectively), along with the corresponding calculated W_{Ao} values, are given in Table II for a series of compositions heated to $T_P = 1140$ °C and Ni-65 wt pct Cu mixtures heated to 1090 °C. The data are also plotted in Figure 4, as a function of the solute content of the bulk specimen (C_O, in wt pct Cu). A theoretical curve corresponding to $W_{Ao} = C_O$ (i.e., the absence of solid-state interdiffusion) is also shown for comparison. As expected, ΔH_m (and, therefore, initial liquid weight fraction W_{Ao}) increases as the Cu content within the mixture increases. However, comparison with the theoretical curve indicates that W_{Ao} is always less than C_O. This clearly indicates that interdiffusion prior to melting occurs and reduces the amount of liquid that initially forms in the powder compact. The overall impact of interdiffusion on the liquid formation is largest at low Cu compositions in which W_{Ao} is less than 50 pct of the C_O value.

Table II. DSC and Density Data for Mixtures Heated to T_p and Immediately Cooled

C_o (Wt Pct Cu)	Temperature T_p (°C)	Preparation Technique (Type)	Endotherm Enthalpy ΔH_m (J/g)	Liquid Fraction $W_{Ao} = \Delta H_m / \Delta H_f$	Density D_{theo}
35	1140	layered/pressed (A)	36.4	0.18	0.87
45	1140	layered/pressed (A)	62.8	0.31	0.92
55	1140	layered/pressed (A)	85.5	0.42	0.95
65	1140	layered/pressed (A)	103.4	0.51	0.96
75	1140	layered/pressed (A)	123.5	0.61	0.98
65	1090	layered/pressed (A)	88.7	0.45	0.92
65	1140	mixed/loose (b)	124.9	0.61	0.96
65	1090	mixed/loose (b)	102.8	0.52	0.92
100	1090	pure Cu mixture—ΔH_f	197.2	1.00	1.00
100	1140	pure Cu mixture—ΔH_f	203.9	1.00	1.00

Metallographic results by Puckert *et al.* for planar arrays of Cu-coated Ni spheres have shown that Ni dissolution occurs at neck regions during TLPS above 1085 °C.[24] Optical macrographs clearly showed increased Ni melting and decreased Ni particle sizes at higher sintering temperatures. Unfortunately, these qualitative observations could not quantify how the liquid fraction was affected. The impact of dissolution on the amount of liquid formed can be determined by comparing the DSC results for the 65 wt pct Cu samples heated to 1090 °C and 1140 °C (Figure 4). At 1090 °C, the liquidus composition is 99 wt pct Cu and, therefore, any dissolution and melting of Cu-rich regions alloyed with Ni will be negligible, in terms of their contribution to liquid formation. By comparison, the liquidus composition at 1140 °C is 92 wt pct Cu. Therefore, the meltback of previously-interdiffused Cu-rich alloyed regions, as well as the Ni dissolution (from increased Ni solubility in the liquid), would be expected to have an impact on the initial liquid formation. A comparison of ΔH_m and W_{Ao} measurements for 65 wt pct Cu type A mixtures at the two temperatures in Table II and Figure 4 clearly indicates that dissolution does cause more liquid to form, increasing ΔH_m from 88.7 J/g (or $W_{Ao} = 0.45$) at 1090 °C (*i.e.*, where no dissolution occurs) to 103.4 J/g (or $W_{Ao} = 0.51$) at 1140 °C. However, it is worth noting that, even at 1140 °C,

Fig. 4—Initial liquid fraction formed (W_{Ao}) for type A and type B brazes heated to 1140 °C and 1090 °C at 40 °C/min.

$W_{Ao} < C_O$, indicating that dissolution does not recover all of the alloyed Cu. Therefore, the Ni regions alloyed below the solidus composition of 86 wt pct Cu at 1140 °C still remain stable in the solid phase and do not melt.

Consolidation. An example of the macrostructures of type A and type B samples sintered at 1140 °C for 0 minutes is shown in Figure 5. Comparing these structures with the same samples heated to 1075 °C (Figure 1) indicates that liquid formation has caused rapid particle rearrangement and increased density within ≤1 minute of liquid duration. This is consistent with TLPS studies of planar arrays of Cu-coated Ni spheres by Puckert *et al.*, which show that the initial densification process occurs by rapid liquid redistribution through capillary action and base metal rearrangement.[24,25] The more segregated starting structure of the compacted type A mixtures has not prevented densification of the sintered material; this again indicates the effectiveness of particle rearrangement. However, increased shape retention is visible in type A mixtures, due to the densely pressed, rigid Ni particle network and decreased liquid fractions indicated by DSC, both of which are less desirable characteristics from the perspective of a flowable braze filler metal. In comparison, the loosely mixed type B mixtures formed more liquid, which was less restricted for Ni particle rearrangement. A comparison of both sintering temperatures for layered/pressed type A mixtures reveals that specimens sintered at 1140 °C appear more distorted, owing to the increased liquid formation. This was less evident in the micrographs for the loose type B specimens, which all showed similar levels of particle rearrangement and shape distortion, owing to the less restrictive loose powder contact. However, it was observed that in both type A and type B types, specimens heated to 1140 °C showed decreased Ni particle sizes, owing to dissolution at higher temperatures, as observed by Puckert *et al.*[24]

Bulk-sintered density measurements were performed on the postsintered type A and type B mixtures *via* the Archimedes method ($\rho_{sintered}$), and these can be expressed as fractions of full density ($D_{theo} = \rho_{sintered}/\rho_{full}$), where full density corresponds to a sintered braze with no voids. These data are plotted in Figure 6, which illustrates how the densification level increases as the initial liquid fraction formed increases. The
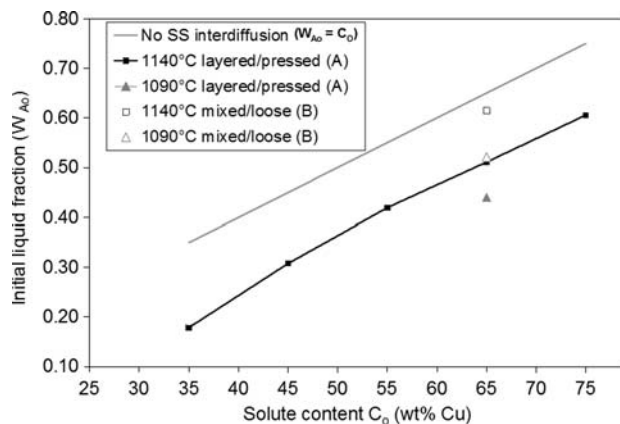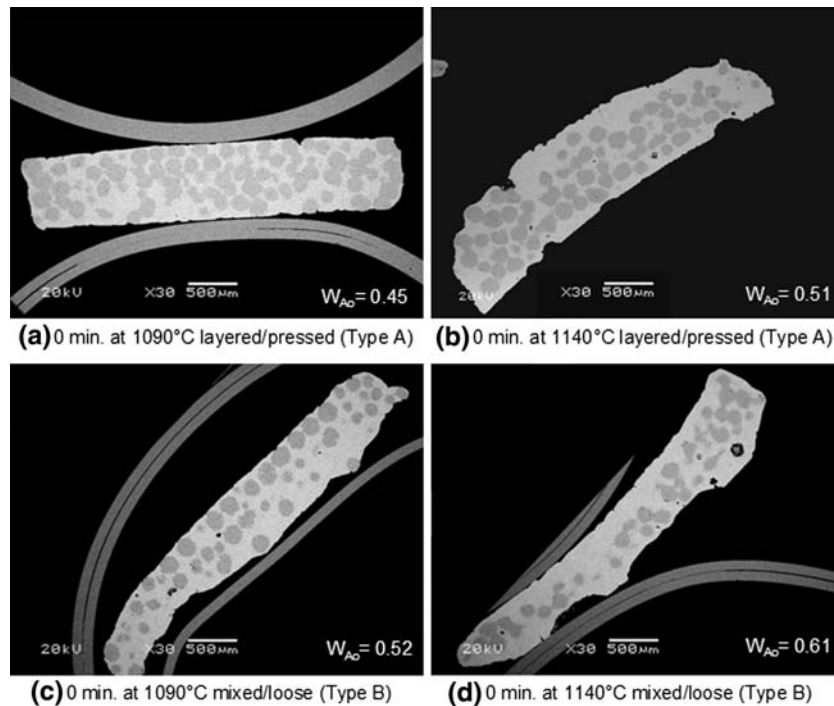
Fig. 5—BSE macrographs of layered/pressed (type A) and mixed/loose (type B) specimens after heating to 1090 °C or 1140 °C and immediately cooled. The initial liquid fraction measured by DSC is identified at the lower right corner.

corresponding C_O values of the specimens shown in Figure 4 are also plotted for each data point. The 1140 °C data shown indicate that type A powder mixtures containing approximately 40 wt pct liquid (*i.e.*, 55 wt pct Cu) or more will have consolidation levels in excess of 95 pct theoretical. Full density was not achieved, even at a high Cu content, due to the presence of residual Ni pores from the starting Ni powder (Figure 2) and large pores within the Cu regions (visible in Figure 5). The large pores associated with liquid regions are likely due to trapped gas. Additionally, unequal diffusivities ($D_{Cu} >> D_{Ni}$) can cause a mass flux imbalance that gradually generates Kirkendall-type "diffusion pores,"[20] which are observed near neck areas,[24,25] and within the Cu-rich regions.[20] However, Kirkendall-type pores are not expected to be the main source of the porosity exhibited in the data of Figure 6, which were collected for after a 0-minute hold at the sintering temperature. These types of pores will make a more significant contribution once greater degrees of interdiffusion have taken place at longer sintering times. Puckert *et al.*[25] as well as Brand and Schatt[20] found that Kirkendall pore formation and swelling became significant with prolonged sintering well after melting and the initial liquid-induced consolidation. An additional influence on the rapid densification upon melting is related to solid-state interdiffusion and dissolution that can be discussed by comparing the consolidation results at 1090 °C and 1140 °C, as described next.

Within the dashed area of Figure 6, data for mixtures of the same bulk composition of Ni-65 wt pct Cu are included. However, differences in the four separate data points include the peak temperature (*i.e.*, 1090 °C and

1140 °C) and preparation technique of the powder mixtures (*i.e.*, layered/pressed *vs* loosely intermixed). It is clear from the figure that, while loosely intermixed powders generate more initial liquid, this does not result in higher sintered densities at the same peak temperature. However, regardless of the mixing method, a peak temperature of 1140 °C always results in higher density. Therefore, density is more sensitive to peak temperature than to liquid fraction or initial powder distribution. This is due to the increased dissolution and meltback of the sintered and interdiffused rigid network created at lower temperatures. This allows more particle rearrangement of the mixture and higher densities.

C. Isothermal Solidification

Based on the DSC data in Figure 6, it was decided to investigate higher-density mixtures (*i.e.*, 65 wt pct Cu) for further isothermal solidification studies. The consolidation levels observed and the significant melting point shift potential of the 65 wt pct Cu mixtures are desirable characteristics for potential VMP braze filler metals. Figure 7 shows DSC traces for 65 wt pct Cu type A specimens heated to 1140 °C, held isothermally for different durations, and then cooled to interrupt the isothermal solidification process. All brazes were found to exhibit very similar endothermic melting peaks at 1085 °C. Upon cooling, solidification peaks that are significantly smaller than the melting peak were found, indicating isothermal solidification of the liquid phase occurred at the processing temperature. Furthermore, traces for samples held for longer times show progressively less liquid solidification. The flat DSC trace for the
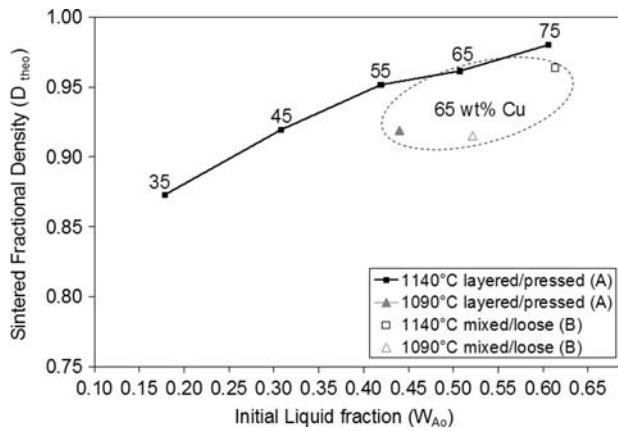
Fig. 6—Fractional density (D_{theo}) *vs* liquid fraction formed for type A and type B brazes heated to 1140 °C and 1090 °C at 40 °C/min.
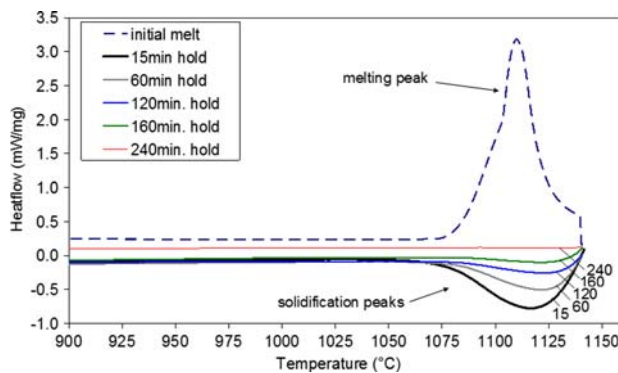

Fig. 7—DSC traces for 65 wt pct Cu type A mixtures heated to 1140 °C, held for different isothermal hold times, and then cooled.

braze held for 240 minutes indicates no liquid solidification upon cooling; therefore, complete isothermal solidification took place between 160 and 240 minutes.

The exothermic solidification energy (*i.e.*, the area under the solidification peaks, ΔH_m), after a certain interrupted isothermal hold time, was quantitatively measured by DSC and Eq. [1] was used to calculate the liquid fraction present (W_A) as a function of hold time t. Figure 8 plots W_A *vs* the isothermal hold time, for mixtures sintered at 1090 °C and 1140 °C. Data sets for type A and type B specimens (*i.e.*, pressed/layered and loose/mixed) are shown in Figures 8(a) and (b), respectively. All data sets illustrate similar transient liquid trends: the large liquid fractions initially formed upon melting are rapidly reduced, with hold time at temperature due to diffusional (or isothermal) solidification. The rate of this solidification (*i.e.*, the slope of each curve) is initially very rapid, but decreases significantly near the end of the solidification process. For the mixed/loose powders (type B), the net solidification rate is more rapid at 1090 °C compared to 1140 °C, resulting in the complete removal of the liquid phase in half the time at the lower temperature. The time required for complete liquid removal is also shorter at 1090 °C, for the layered pressed powders (type A). However, the times for complete liquid removal are similar at both temperatures for type A mixtures, and are considerably longer than that measured for the mixed/loose counterparts. These data will be further discussed in Sections III–E and F.

Microstructural evidence of the isothermal solidification mechanism. After prolonged sintering, it was found that all specimens exhibited still-distinguishable Ni-rich particles (Figure 5) and a gradual increase in fine Kirkendall-type pores near the previous interface (*i.e.*, the high interdiffusion region). Useful quantitative information regarding the degree of interdiffusion within the cooled/solidified, single-phase DSC specimens can be obtained by measuring compositional gradients *via* EDS (in wt pct Cu). This technique can provide an improved understanding of the diffusional (or isothermal) solidification process, by examining the evolving distribution of solute in the base metal particles and in the adjacent isothermally-solidified regions. Figure 9 shows quantitative compositional profiles originating at the Ni particle cores and progressing radially to the peripheral Cu-rich regions, for mixed/loose samples at 1090 °C and 1140 °C (similar results were obtained for particles within layered/pressed type A samples). A range of hold times during the isothermal step, as well as a profile from a sample heated to just below the point of melting (*i.e.*, 1075 °C), are included in the plot. These data were obtained by EDS spot analysis consisting of radially-aligned analysis points at 10-μm increments from the Ni core (at $r = 0$ μm). All efforts were made to minimize positional errors by analyzing similarly-sized, spherical particles (*i.e.*, radius $a \sim 80.5$ μm).

For both the 1090 °C and 1140 °C data sets shown in Figure 9, the profiles obtained for specimens prior to melting show some Cu penetration in the Ni particle (and *vice versa*), as well as a sharp compositional gradient near the original interface. This is consistent with the solid-state interdiffusion evidence given in Figure 2. A uniform concentration of approximately 100 wt pct Cu is found in the unmelted Cu regions. Immediately after melting at 1090 °C (0 minutes, curve in Figure 9(a)), the frozen liquid composition is still quite uniform and was measured to be approximately 99 to 100 wt pct Cu, corresponding to the equilibrium liquidus at 1090 °C (C_L). After initial melting at 1140 °C (0 minutes, curve in Figure 9(b)), the frozen liquid regions are shown to have rapidly obtained uniform compositions near 92 to 93 wt pct Cu (≤1 minute), due to high diffusivity rates in the liquid. This is also consistent with the equilibrium liquidus composition at 1140 °C. Interfacial compositions constrained by local equilibrium at C_S/C_L were also observed by Puckert *et al.* in the Ni/Cu system,[23] where C_S is given by the phase diagram solidus at T_P.

The data of Figure 9 indicate that, even at a 0-minute hold time, a large portion of the Cu-rich microstructure has obtained a Cu concentration at or below C_S, suggesting that it isothermally solidified (*i.e.*, it has a composition within the single-phase solid region of the Ni-Cu phase diagram). For example, at 1090 °C and 1140 °C, a concentration of $C < C_S$ occurs at the radial positions of 150 and 130 μm, respectively. These
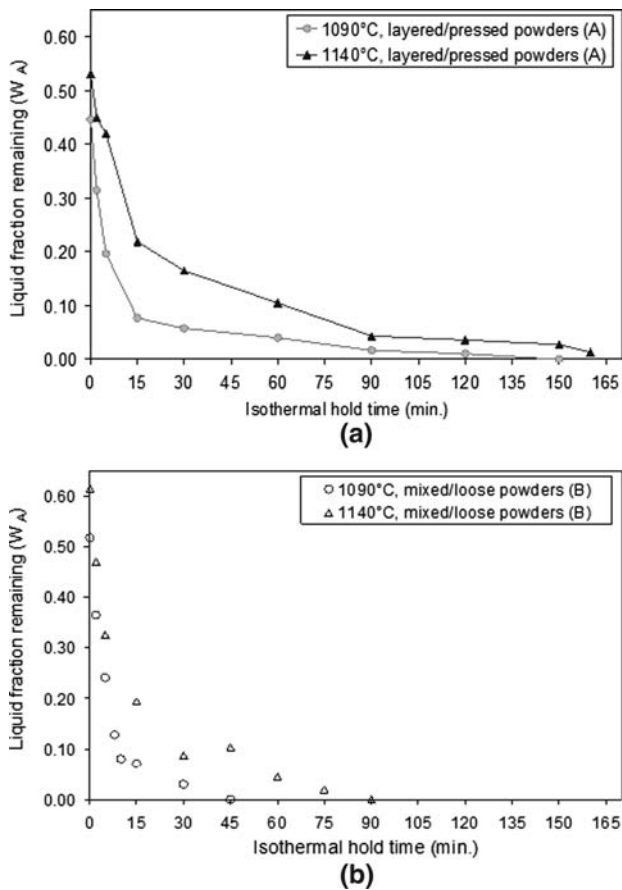
Fig. 8—DSC results showing the fraction of liquid remaining after interrupted isothermal holds at 1090 °C and 1140 °C for 65 wt pct Cu mixtures: (a) layered/pressed mixtures (type A) and (b) mixed/loose mixtures (type B).

solid-solution regions are larger than the initial Ni particle radius of 80.5 μm and support the diminished initial liquid-formation measurements of Figure 4 (i.e., $W_{Ao} < C_O$). Furthermore, the relatively larger $C < C_S$ solid-solution region at $t = 0$ minutes for 1090 °C vs 1140 °C in Figure 9 (~150 vs 130 μm) is consistent with the decreased initial liquid fraction (or increased solid fraction) measured by DSC at 1090 °C. The curves at successively longer hold times show decreased Cu

contents at longer radial distances from the Ni core. This is a result of solute diffusion across the moving solid-liquid interface and into the isothermally-solidified regions. For the 30-minute hold data at 1090 °C and 1140 °C, compositions close to C_L remain at radial distances of 150 μm and above. This indicates the continued presence of liquid phase in these samples, which is consistent with the DSC results of Figure 8. After 45 minutes at 1090 °C and 75 minutes at 1140 °C, all compositions were measured below C_S, indicating complete isothermal solidification. These results are also consistent with the DSC measurements of Figure 8, given that the DSC measures bulk behavior, whereas the EDS results are for isolated particles.

It is interesting to note from Figure 9 that Cu penetration deeper into the Ni base metal particle is slow and the Cu concentration gradients near the original interface ($r = 80$ μm) remain sharp, even at long hold times. This stepped solute profile indicates the lack of long-range diffusion into the Ni core, which remains very Ni rich during isothermal solidification, even when no liquid exists after 75 minutes at 1140 °C. Furthermore, a fairly Cu-rich "layer" has formed surrounding base metal particles; this layer has Cu-rich compositions close to C_S. This suggests that the isothermal solidification of the liquid primarily occurs by epitaxial growth of the alloyed base metal particles via the progression of the solid-liquid interface, which leaves behind a Cu-rich solid-solution that is constrained at C_S by local equilibrium at the moving interface.

D. Homogenization and Reheating

Three layered/pressed powder mixtures were selected for reheating experiments, to study the influence of the hold-time duration on the degree of homogenization and melting point shift. For these experiments, samples were initially heated to 1140 °C and underwent ~100 pct isothermal solidification after different hold-segment durations (i.e., 150, 240, and 360 minutes). They were then cooled to room temperature and reheated well past the liquidus temperature of the bulk mixture composition (1300 °C), to cause complete remelting, and then finally cooled again to room temperature. The reheat profiles of these samples after the isothermal holds at
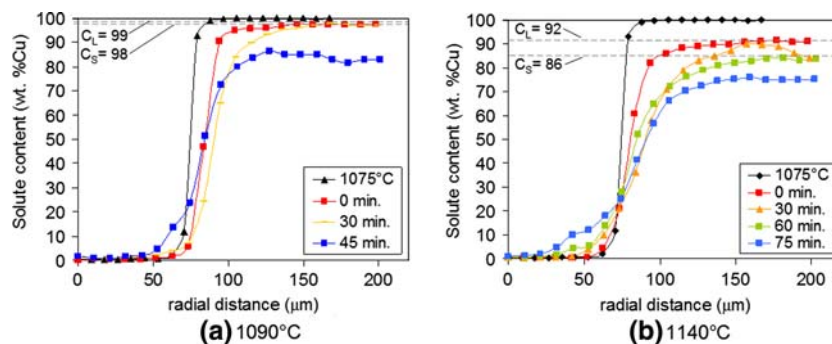

Fig. 9—Evolution of radial concentration profiles from the Ni core, measured by EDS for 65 wt pct Cu TLP sintered loose/mixed specimens (type B): (a) 1090 °C and (b) 1140 °C.
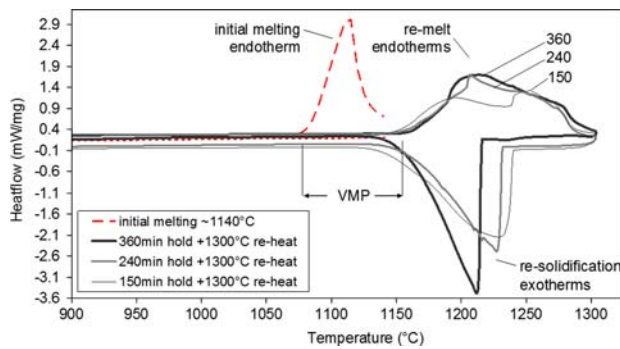
Fig. 10—DSC traces for 65 wt pct Cu pressed/layered mixtures (type A) that were reheated to 1300 °C, showing different melting point shifts and degrees of homogenization.

Table III. Melting Point Shift Data for Layered/Pressed Mixtures (Type A)

Hold Time at 1140 °C (Min)	New Melting Point (°C)	Melting Point Shift (°C)	Melting Range (°C)
150	1150.0	65.1	140.8
240	1157.2	72.3	135.6
360	1168.7	83.8	132.1

1140 °C are shown in Figure 10. Also included for comparison is a heating segment showing the initial melting behavior of the powder mixtures at 1085 °C. The melting endotherms during the reheat segments of all three specimens indicate higher onset temperatures, which correspond to melting point shifts. The reheated melting endotherms are also much broader than the initial melting endotherms, due to compositional gradients. Table III shows the measured remelt onset temperatures for these three samples, as well as the corresponding melting point shifts and melting ranges.

The broad melting range of these reheated TLP sintered brazes is due to incomplete homogenization of the isothermally-solidified powder mixtures, as evidenced by the EDS compositional profiles in Figure 9. This causes progressive melting through compositional gradients within the specimen, as the temperature is increased during reheating. The steplike EDS compositional profiles observed at the end of isothermal solidification clearly explain why the reheat DSC traces for the 150-minute specimen contained a double peak. Remelting first consisted of melting the peripheral Cu-rich regions, which was followed by melting of the Ni-rich core region at higher temperatures. In comparison, the 240- and 360-minute DSC traces show single-peak melting endotherms that are progressively narrower, due to increased homogeneity.

IV. DISCUSSION

A. Temperature Effects

The results just discussed for the various TLPS stages can be discussed with the aid of a conceptual model

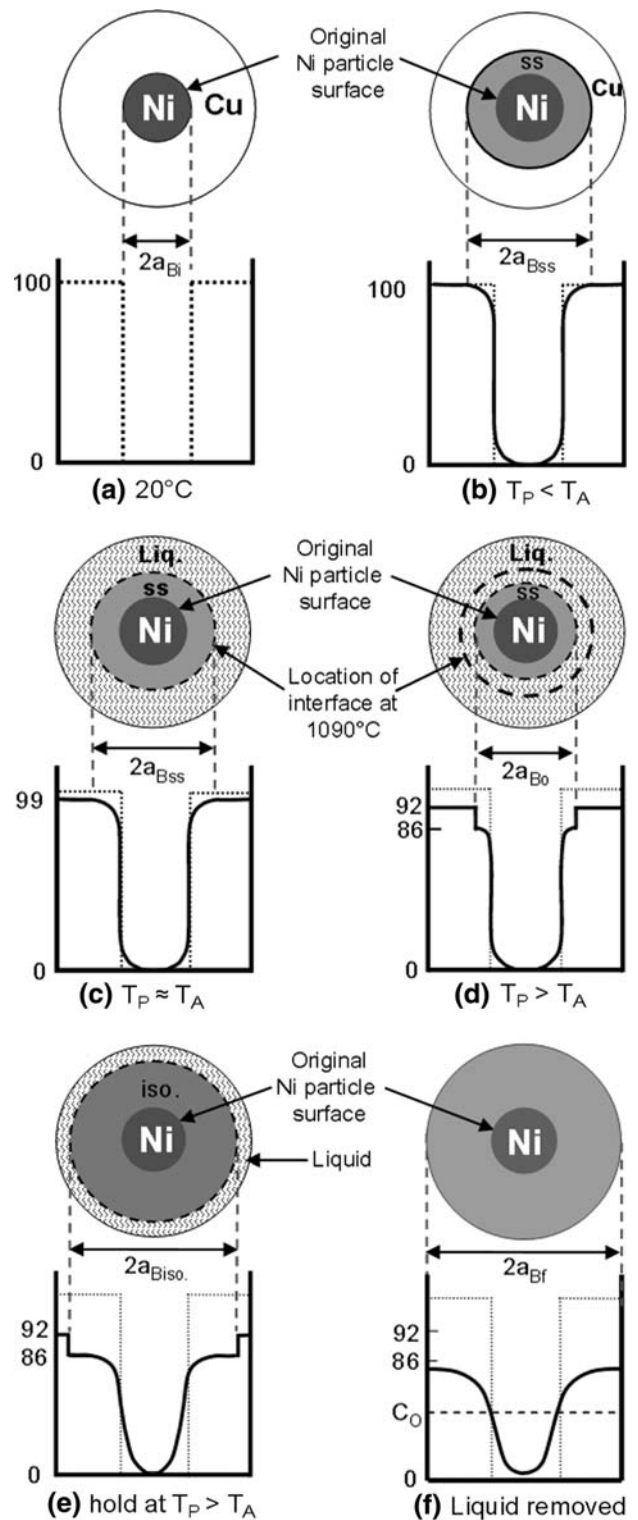Fig. 11—Simplified concentric sphere model showing solid/liquid fractions and solute concentration profile evolution during TLPS.

illustrated in Figure 11, which depicts a base-metal Ni particle having an initial radius a_{Bi} surrounded by a pure Cu matrix. This concentric-sphere model is a reasonable assumption for a representative unit cell, particularly for the pressed powder compacts, because the particle size

of Ni is much larger than the Cu powder.[18,23,24] The effects of the developing Kirkendall-type pore structure and interparticle densification will not be discussed, in order to simply illustrate the liquid removal process within a single unit cell. However, the developing Kirkendall pore structure will affect the diffusion field, by decreasing the density and connectivity of the couple, thereby decreasing mass transport rates and isothermal solidification kinetics.

Prior to heating, no interdiffusion between the as-received powders is shown by the square, dashed profile in Figure 11(a). During athermal heating to process temperatures $T_P \leq T_A$ (T_A being the melting point of the additive phase, Cu (1085 °C)), a solid-state-sintered interdiffusion region and profile develops (the dark solid curve and the solid gray phase labeled SS, having radius a_{Bss} in Figure 11(b)).

Once $T_P \approx T_A$ (e.g., 1090 °C), only the most Cu-rich regions of the solid-state-sintered profile having compositions ranging from C_L to pure Cu (99 to 100 wt pct Cu) will melt (illustrated by the hatched "Liq." region in Figure 11(c)). The solid-liquid interface is represented by a dashed circle and the diameter of the bounded solid-solution region (i.e., the new solid particle with radius a_{Bss}) is extended onto the compositional gradient below. At $T_P \approx T_A$, essentially no Ni dissolution or liquid dilution occurs, because $C_L = 99$ wt pct Cu (i.e., negligible Ni solubility in the liquid phase). As DSC results have quantitatively shown, this results in a decreased initial liquid fraction ($W_{Ao} < C_O$ in Figure 4). Figure 11(c) illustrates how this diminished liquid fraction via solid-state interdiffusion results in an enlarged, solid-state-sintered Ni particle, in comparison to its original size (i.e., $a_{Bss} > a_{Bi}$). The EDS results have also shown that the liquid rapidly (≤ 1 minute) obtains a uniform, saturated compositon at C_L, due to high diffusivity rates within the liquid phase.

For the case in which $T_P > T_A$ in Figure 11(d) (e.g., 1140 °C), the dissolution and melting of the outer regions of the Ni particle serve to decrease the Ni particle size to a_{Bo}, at the beginning of the isothermal segment. As evidenced by the DSC results, this serves to recover some of the liquid lost due to solid-state sintering, because a portion of the solid-state-sintered regions (labeled SS), having solute contents above the new solidus C_S (i.e., > 86 wt pct Cu at 1140 °C), now melt, as they are nonequilibrium regions at $T_P > T_A$. This recovered liquid phase is illustrated by the liquid region surrounding the diminished SS region and inside the heavy dashed line of Figure 11(d), which represents the previous 1090 °C interface at a_{Bss}. Also, the increased solubility of Ni in the liquid phase, as indicated by the new equilibrium liquidus composition ($C_L = 92$ wt pct Cu at 1140 °C) leads to dissolution of the Ni particles and dilution of the liquid to a lower C_L. The interfacial solid-surface concentration of the Ni particles at $T_P = 1140$ °C is also reduced, from $C_S \approx 99$ wt pct Cu at 1090 °C to the new solidus concentration of 86 wt pct Cu at 1140 °C. The solute profile in the particles is altered accordingly and resembles those measured by EDS in specimens shortly after melting.

With the hold time at the process temperature of 1140 °C, isothermal solidification takes place by the movement of the solid-liquid interface outward and the growth of the Ni particle (Figure 11(e)). The DSC data have shown that this is evidenced as a measurable decrease in the liquid fraction with increasing hold time. As the EDS analysis of Figure 9 indicates, the isothermal solidification process creates a Cu-rich solid shell surrounding the original Ni particle (the solid region labeled as "iso" in Figure 11(e)); this shell has compositions near C_S with very little long-range diffusion into the particle core. The growth of particle via this relatively saturated peripheral region, which has small compositional gradients (i.e., low diffusion, mass transfer rates), explains the slower solidification kinetics at long hold times (Figure 8). Grain growth, overlapping unit cells, particle growth and saturation, and the developing Kirkendall pore structure will further slow mass transfer and diffusional solidification rates. Finally, when all of the liquid is removed from the sample (i.e., Figure 11(f)) the solid-liquid interface is no longer present and the composition of the Cu-rich outer region

Table IV. DSC Liquid Fraction Data as a Function of Hold Time at 1090 °C and 1140 °C for Type A and B Mixtures

| | Liquid Fraction Remaining (W_A) | | | |
| | Layered/Pressed (A) | | Mixed/Loose (B) | |
Isothermal Hold Time (Min)	1090 °C	1140 °C	1090 °C	1140 °C
0	0.45	0.51	0.52	0.61
2	0.31	0.44	0.37	0.47
5	0.20	0.42	0.24	0.33
15	0.08	0.22	0.07	0.19
30	0.06	0.16	0.03	0.09
60	0.04	0.10	0.00	0.04
90	0.02	0.04	—	0.00
120	0.01	0.04	—	—
150	0.00	0.03	—	—
160	—	0.01	—	—
240	—	0.00	—	—

will drop below C_S, because it is no longer constrained by local equilibrium with the liquid. As depicted in Figure 11(f) (and evidenced by the EDS results of Figure 9), even at this stage the center of the Ni particle only contains a few wt pct Cu. Homogenization within the solid-solution structure serves to gradually decrease concentration gradients with increasing hold time. At $t = \infty$, the sintered mixture will obtain a uniform composition determined by the bulk mixture composition (the dashed line at C_O in Figure 11(f)).

B. *Liquid Distribution*

The DSC results from Figure 8 are tabulated in Table IV, to evaluate the effects of liquid distribution caused by the different preparation techniques. Both layered/pressed data sets in Table IV required much more time to completely solidify the liquid phase when compared to the mixed/loose data. Yet, in the 1140 °C case, for example, the liquid fractions of layered/pressed specimens after 2 minutes are somewhat smaller than those of the mixed/loose specimens. This is likely due to the fact that, although Ni-Cu distribution is more segregated in the layered/pressed compacts, pressing counteracts this effect by significantly increasing the deformed contact area between the powders. This increases solid-state interdiffusion and reduces initial liquid fractions relative to type B mixtures at both temperatures. Figure 8 shows that, as hold time increases, the rate of isothermal solidification slows significantly in layered/pressed type A specimens, due to the less homogeneous liquid distribution around the densely-compacted Ni skeleton network. As the isothermal process continues, the layered/pressed and mixed/loose curves progressively deviate/separate. After approximately 30 minutes, the layered/pressed type A samples now contain almost 50 wt pct more liquid in comparison. This difference becomes more pronounced at long hold times, when layered/pressed samples required over an additional hour for complete isothermal solidification at both temperatures, indicating a slower net isothermal solidification process.

In summary, pressing may explain the somewhat smaller initial liquid fractions, but the increased inhomogeneity in the layered/pressed samples explains the prolonged solidification times required. Relative to the pressed samples, liquid distribution and particle rearrangement are less restricted in the loose mixtures. The less-uniformly-distributed liquid formations in type A samples creates certain liquid-deficient areas that will solidify rapidly due to a relative abundance of adjacent Ni particles (as found at short hold times). Conversely, larger liquid ''pools'' found in peripheral areas of the specimens will require much more time to be removed by solute diffusion into the few adjacent base metal particles. This effect is amplified by green pressing, because flow and uniform redistribution of the liquid is inhibited by the pressed and sintered Ni skeleton. These observations can be made at both temperatures studied, where slow, prolonged solidification is particularly evident at long hold times.

V. CONCLUSIONS

It was found that DSC is a useful tool for quantitatively determining liquid fractions during TLPS. When combined with microscopy techniques, important observations can be made about the evolving macrostructure, microstructure, and solute distribution. Sintered specimens showed that braze densities above 95 pct could be achieved with Cu concentrations of 55 wt pct or higher. Full densification did not occur, due to observed large trapped gas pores, residual starting Ni powder pores, and Kirkendall pores generated from unequal diffusivities. For 65 wt pct Cu loose powder mixtures, complete isothermal solidification of the liquid at a processing temperature of 1140 °C occurred in approximately 90 minutes. However, solidification of the liquid phase for identical braze mixtures sintered at 1090 °C occurred in significantly less time (45 minutes). This can be explained by the observed increase in liquid fractions formed at higher processing temperatures (due to the dissolution of Ni), which effectively counteracts the increased diffusivities at these temperatures and requires more time to isothermally solidify. Green-pressed and layered brazes required much more time for complete isothermal solidification, due to inhomogeneous liquid distributions. The increase in the postprocessed melting point of this braze composition (65 wt pct Cu) was in excess of 80 °C upon reheating. The DSC, SEM, and EDS data suggest that isothermal liquid solidification occurs by limited long-range Cu diffusion within the Ni particles, which grow epitaxially by the transient progression of the solid/liquid interface at compositions given by the liquidus and solidus.

REFERENCES

1. R. Ventkatraman, J.R. Wilcox, and S.R. Cain: *Metall. Mater. Trans. A*, 1997, vol. 28A, pp. 699–706.
2. P. Gandhi, C. Gallagher, and G. Matijasevic: *J. Electron. Manuf.*, 1997, vol. 7, pp. 253–60.
3. M.A. Palmer, C.N. Alexander, and B. Nguyen: *J. Electron. Mater.*, 1999, vol. 28, pp. 912–15.
4. T. Studnitzky and R. Schmid-Fetzer: *J. Electron. Mater.*, 2003, vol. 32, pp. 70–80.
5. X. Qiao and S.F. Corbin: *Mater. Sci. Eng.*, 2000, vol. A283, pp. 38–45.
6. S.F. Corbin and P. Lucier: *Metall. Mater. Trans. A*, 2001, vol. 32A, pp. 971–78.
7. S.F. Corbin and D.J. McIsaac: *Mater. Sci. Eng. A*, 2003, vol. A346, pp. 132–40.
8. E. Lugscheider, T.H. Schittny, and E. Halmoy: *Weld. J.*, 1989, vol. 68 (1), pp. 9s–13s.
9. W.F. Gale, D.A. Butts, M. Di Ruscio, and T. Zhou: *Metall. Mater. Trans. A*, 2002, vol. 33A, pp. 3205–14.
10. B. Rieger, W. Schatt, and C.H. Sauer: *Int. J. Powder Metall. Powder Technol.*, 1983, vol. 19 (1), pp. 29–41.

11. R.G. Iacocca: *Metall. Mater. Trans. A*, 1996, vol. 27A, pp. 145–53.
12. A. Lal, R.G. Iacocca, and R.M. German: *Advances in Powder Metallurgy and Particulate Materials—1996*, Metal Powder Industries Federation, Princeton, NJ, 1996, pp. 11289–11298.
13. A. Lal, R.G. Iacocca, and R.M. German: *Metall. Mater. Trans. A*, 1999, vol. 30A, pp. 2201–08.
14. A. Lal, R.G. Iacocca, and R.M. German: *J. Mater. Sci.*, 2000, vol. 35, pp. 4507–18.
15. R.M. German: *Liquid Phase Sintering*, Plenum Press, New York, NY, 1985.
16. R.M. German: *Sintering Theory and Practice*, Wiley-Interscience, New York, NY, 1996, pp. 373–95.
17. R.N. Lumley and G.B. Schaeffer: *Scripta Mater.*, 1996, vol. 35, p. 589.
18. S.F. Corbin: *Metall. Mater. Trans. A*, 2002, vol. 33A, pp. 117–24.
19. W.H. Baek and R.M. German: *Int. J. Powder Metall.*, 1986, vol. 22 (4), pp. 235–44.
20. K. Brand and W. Schatt: *Z. Metallkd.*, 1993, vol. 84 (12), pp. 893–98.
21. D.J. Lee and R.M. German: *Int. J. Powder Metall.*, 1985, vol. 21 (1), pp. 9–21.
22. A.P. Savitskii: *Liquid Phase Sintering of Systems with Interacting Components*, Institute of Strength Physics and Materials Science, Tomsk, Russia, 1993, pp. 16, 53–60.
23. D.M. Turriff and S.F. Corbin: *Metall. Mater. Trans. A*, 2006, vol. 37A, pp. 1645–55.
24. F.J. Puckert, W.A. Kaysser, and G. Petzow: *Z. Metalkd*, 1983, vol. 74 (11), 737–43.
25. F.J. Puckert, W.A. Kaysser, and G. Petzow: *Sci. Sintering*, 1984, vol. 16, pp. 105–13.